Check for updates

A high-performance TiO$_2$ nanowire UV detector assembled by electrospinning

Yuting Wang, [ID] Jing Cheng, [ID] Muhammad Shahid, Mengfei Zhang and Wei Pan*

Here, a transparent, flexible and nanoscale TiO$_2$ ultraviolet (UV) photodetector has been fabricated by electrospinning. Well aligned TiO$_2$ nanowires were collected on a flexible mica substrate. Then, the nano-device was simply assembled by depositing interdigitated platinum electrodes on the surface. Upon UV illumination, the photosensitivity of this device is up to over three orders of magnitude with relatively fast and stable response speed under 254 nm and 365 nm UV light. This nanosensor retains a high photo-dark current ratio, fast response time and stable durability during bending tests, indicating an excellent reversibility and stability of the flexible TiO$_2$ nanowires. The highly flexible photosensor demonstrates a good potential candidate for wearable optoelectronic applications.

1. Introduction

Flexible or stretchable electronic devices with high mechanical stability are considered key components for next generation wearable smart electronics.[1–3] Although inorganic-based semiconducting nanomaterials present excellent UV sensitivity and fast response/recovery speed,[4] the poor flexibility of ceramic materials hinders their wide application.[5] Flexible photodetectors based on bendable plastic substrates have attracted great attention because of their potential applications in optoelectronics, sensors, and transducers, etc.[3,6,7] Among various ceramic oxides, titanium dioxide, as an n-type semiconductor with a wide bandgap (anatase 3.2 eV and rutile 3.0 eV), is well known for its versatile characteristics in photocatalysis, solar cells, and diodes etc.[8–11] In particular, TiO$_2$ has been widely used in photocatalysis because of its outstanding photocatalytic activity and electronic properties.[12–17] Many nanotechniques have been developed to fabricate one-dimensional (1D) TiO$_2$, such as nanorods,[18] nanowires,[19] nanobelts,[20] and nanotubes.[21] Three crystal phases of TiO$_2$ are well known as rutile, anatase, and brookite.[22] Although the bandgap energy for anatase phase (∼3.2 eV) is larger than the rutile (∼3 eV), it shows high photocatalytic activity and efficiency of the charge carrier photogeneration when combining anatase and rutile mixtures of TiO$_2$ nanocrystalline with a radio of 80% and 20%.[23,24] As we known, few research has reported about the photoresponse performance of TiO$_2$-based photodetector.

Electrospinning is a facile approach to produce one-dimensional (1D) nanostructures with great scalability. The diameter and morphology of the electrospun nanofibers could be simply controlled by adjusting the density of precursor solutions, applied voltage, working distance and spinning rate.[25] Moreover, this nanomaterial synthesize technology shows advantages of low cost, high efficiency and convenient assembly. Electrospun nanofibers demonstrate outstanding electric, optic, mechanical and magnetic flexibility properties, with considerable potential for novel applications in different fields.[26–29] However, most of the reports for electrospun nanofibers concentrated on the 1D nanostructures. More detailed research on the fabrication of two-dimensional (2D) networks has not been reported so much. Actually, the collected eletrospun nanowires could be automatically formed as a nanoweb on the plate substrate. Therefore, in this study, electrospinning was used for fabricating ultralong nanowires and flexible 2D nanowebs by simply annealing these 2D networks in air.

Here, we report a high-performance 2D nanoweb photosensor composed of ultralong 1D-structured TiO$_2$ nanowires. The nanoweb-based photodetector shows high photo-dark current ratio, excellent mechanical flexibility and durability. Possible mechanisms of the improved mechanical performance of this TiO$_2$ nanosensor have been discussed in detail.

2. Experimental section

TiO$_2$ nanowires were synthesized using an electrospinning approach. Tetrabutyl titanate (6 wt% of the ceramic precursor) was first dissolved in the mixture of ethanol–acetic acid (3.3 : 1, volume rate). After stirring for 30 min, a concentration of 6 wt% polyvinylpyrrolidone (PVP, MW = 1 300 000) was further mixed to control the viscosity. Afterward, the prepared solution was stirred at room temperature for 2 h to achieve complete dissolution and mixing. After dissolution of all the components, the obtained transparent precursor solution was placed in a hypodermic syringe at the positive voltage of 15 kV with a constant flow rate of 0.5 mL h^{-1}. The distance between the needle tip and

State Key Laboratory of New Ceramic and Fine Processing, School of Materials Science and Engineering, Tsinghua University, Beijing 100084, P. R. China. E-mail: panw@mail.tsinghua.edu.cn; Fax: +86-10-62771160; Tel: +86-10-62772858

the aluminum foil collector was 15 cm. Finally, nanofiber webs were removed from the collector and annealed in air at different temperatures, 550 °C, 600 °C, 700 °C, and 800 °C for 1 h with the heating rate of 5 °C min^{-1}, respectively.

The morphologies of TiO_2 nanowires and flexible nanowebs were observed by scanning electron microscopy (SEM, JEOL JSM-6460LV, Tokyo, Japan) and transmission electron microscopy (TEM, JEOL-2011, Tokyo, Japan). A diffractometer (XRD, D/max-2500, Rigaku Co., Tokyo, Japan) was used to examine the crystal structures of these samples. The current–voltage (I–V) characteristics of TiO_2 networks were measured by a Keithley (4200 system, Cleveland, OH, USA). Moreover, the photoresponse characteristics of the UV detectors were monitored using UV light (Philips TUV 8 W, 254 nm, an average power density of 0.5 W cm^{-2}).

3.   Result and discussion

Intuitively, the flexible photosensor consists of semi-conductive nanowires and platinum electrodes, shown in Fig. 1a. By electrospinning, continuous aliened TiO_2 nanowires are first collected on a flexible and transparent mica substrate. Pt electrodes were deposited using a mask by high quality vacuum evaporation. Fig. 1b shows a photograph of the flexible sensor attached to a nonplanar surface. The morphology and

microstructures of highly oriented TiO_2 nanowires were observed by SEM (Fig. 1c and d). Ultra-long TiO_2 nanowires preserve their continuity after 1 h annealing under air. Magnified image shows smooth surfaces and a uniform diameter of $\sim$200 nm of the nanowires. The smooth surface and continues structure of these nanowires reveal that they would have more uniform strength and thus more easily to release the strain compared with fibers of rough surfaces and short lengths upon bending. The TEM image in Fig. 1e also shows a fibrillar structure and a smooth surface of the annealed TiO_2 nanowire. A selected-area electron diffraction (SAED) pattern shown in the inset of Fig. 1e reveals that the nanofibers are comprised of polycrystalline and fine grains with no preferential orientation. Fig. 1f shows a high-resolution transmission electron microscopy (HRTEM) image with distances of crystal lattice fringes of 3.5 Å that can be attributed to the spacing of (101) lattice plane of the anatase TiO_2.[30]

Ultra-long TiO_2 nanowires can be further assembled to a two-dimensional nanopaper. This free-standing nanopaper could be bended without any cracking. SEM measurements were used to determine the strength of TiO_2 nanoweb. Fig. 2a and b show the distinct boundary of the folded nanopaper. The TiO_2 nanofibers are not broken or got any fracture when bended in half. Moreover, spring- and wave-like structures have been spontaneous formed during eletrospinning.[31] After annealing, the spring-like nanowires could maintain their curly and wavy geometries, attributing to the superior mechanical flexibility of TiO_2 nanomaterials. Fig. 2d shows that the freestanding TiO_2 networks are successfully folded in half and remain intact. The mechanistic explanation is that the TiO_2 nanowires remain continuous and undergo nano-scaled deformation to relax the applied stress upon folding.

To investigate the crystal structure of the nanofibers, X-ray diffraction (XRD) analyses of TiO_2 nanofiber-based powders were observed after annealing at 500 °C, 550 °C, 600 °C, 700 °C, and 800 °C for 1 h in Fig. 3. The as-spun nanofibers are amorphous in nature, and the polycrystalline nanofibers are formed after calcination at 500 °C. We note that the annealing temperature could distinctly affect the phase compositions of the TiO_2 nanowires. As the sample is calcined at 500 °C, a phase occurs with a low and wide characteristic peak corresponding to the typical anatase crystal, and this phase completely disappears at 800 °C, leaving pure rutile phases. The XRD patterns also show a mixture of anatase and rutile phases in the annealing range of 500 to 700 °C. It proves that the different ratio of these two phases in TiO_2 composite could be simply controlled by annealing at different temperatures. Contrasting the strength of the anatase (101) peak and the rutile (110) peak in Fig. 3, the concentration of anatase phase in hybrid TiO_2 nanofibers can be estimated as 92%, 83%, 75%, 17%, and 6%, corresponding to the annealing temperature change from 500 to 800 °C, respectively. It was reported that anatase TiO_2 shows more photocatalytic activity than its rutile phase due to its large surface area,[24,32] thus, in this study, the high-performance TiO_2 nanosensor is composed of a majority of anatase phases combined with little amount of rutile phases. With the high reactivity of anatase TiO_2 together with the lower band gap of rutile TiO_2, the process of the
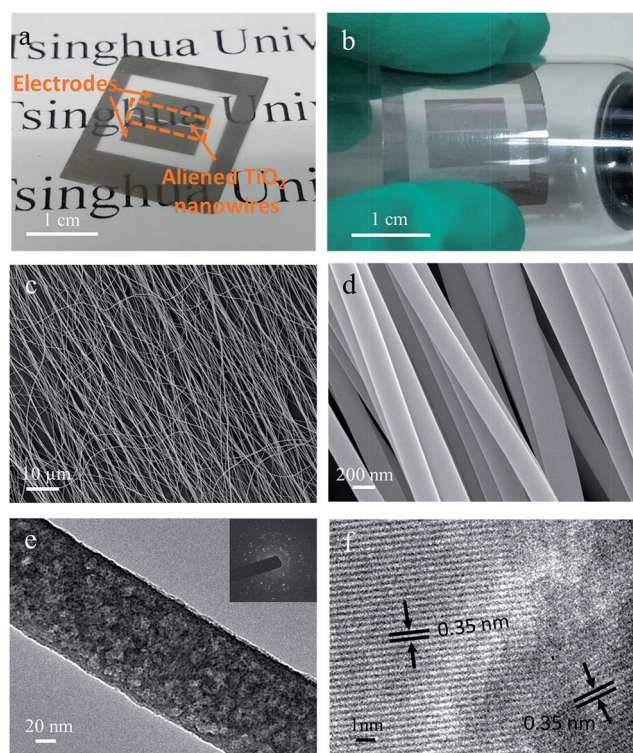

Fig. 1 Highly oriented TiO_2 nanowire photosensor. (a) Schematic representation of the device assembled by aliened TiO_2 array and coated Pt electrodes. (b) Photograph of the photosensor attached to curved surface. (c and d) SEM images of highly oriented TiO_2 nanowires. (e and f) TEM and HRTEM images of the TiO_2 nanowire annealed to 550 °C. The inset shows the SAED pattern.
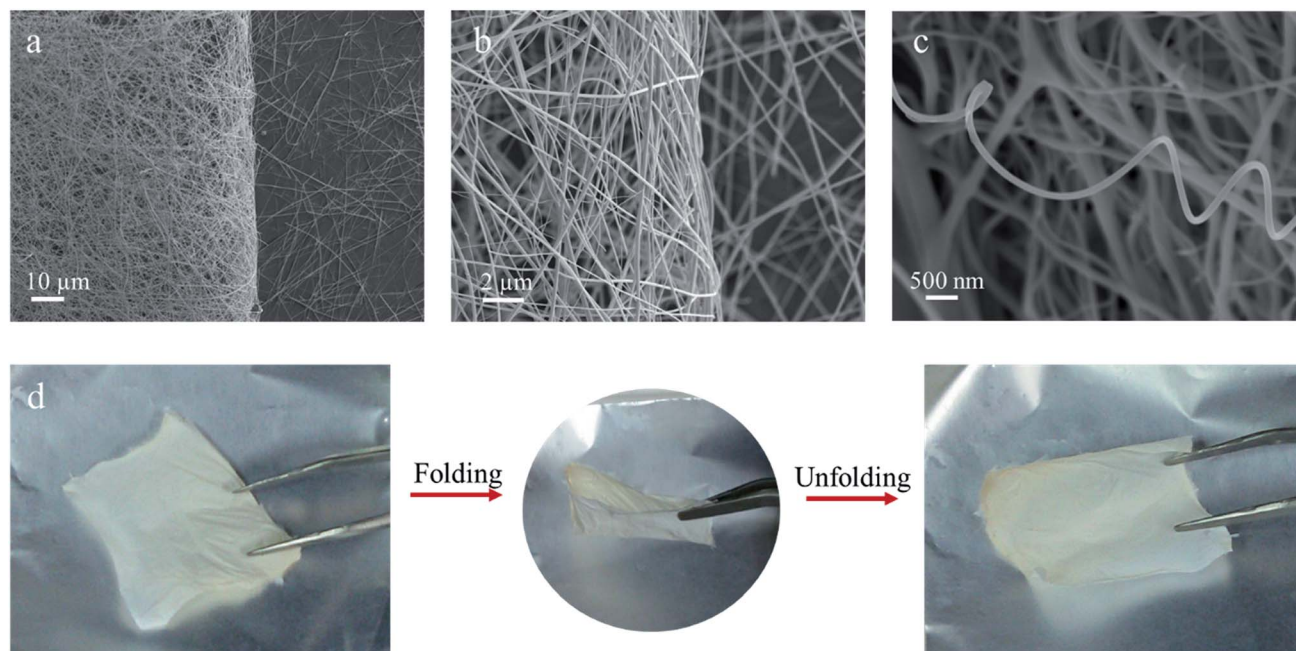
Fig. 2 Flexible TiO_2-based ceramic nanopapers. (a and b) SEM images of the flexible nanopaper folded in half. (c) SEM image of a spring-like TiO_2 nanowire. (d) Photographs of TiO_2 network-based ceramic nanopaper under folding and unfolding.

photoinduced electrons and holes transfer between conduction and valence bands can be highly facilitated in the composite sample.

The mechanism of phase-dependent photoresponse activity in phase junction TiO_2 nanowires is drawn in Fig. 4a. The band gaps of anatase and rutile phases of TiO_2 are 3.2 and 3.0 eV, respectively. This means that when the two phases are in nano-contact there will be a phase junction between the band edges. The phase junctions can promote charges transfer from anatase to rutile phases, similar to the mechanism of P25.[24,33] When the photosensor is illuminated under UV light with photon energy higher than the band gap of anatase TiO_2, electrons in the
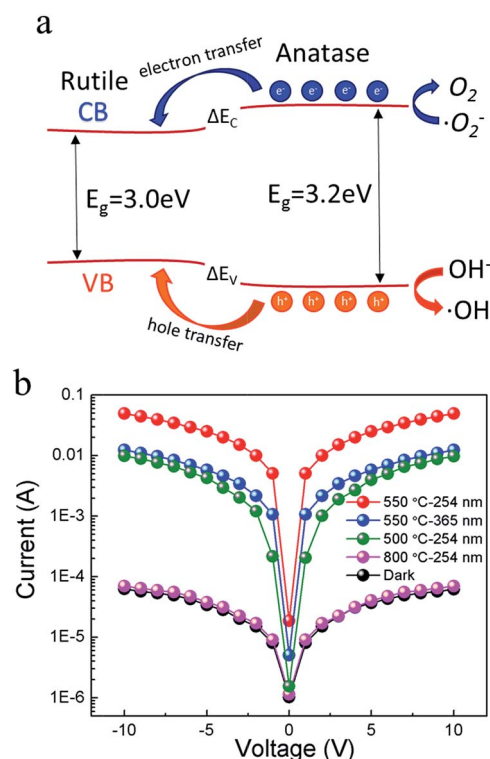

Fig. 3 XRD patterns of a TiO_2 nanowires annealed at different temperatures.

Fig. 4 (a) Schematic illustration of the band structure related mechanism for the anatase/rutile TiO_2 phase junction. (b) $I-V$ curves of the flexible TiO_2 photodetector calcined at 500, 550 and 800 °C under dark or different light illuminations; the incident light power density = 500 μW cm^{-2}.
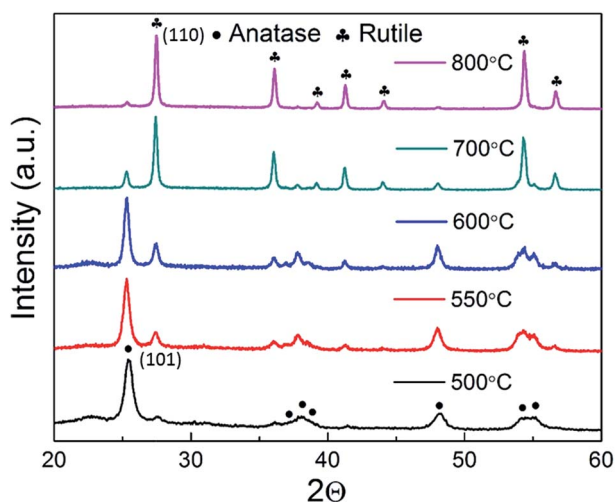
valence band can be excited to the conductive band with the generation of the same amount of holes. Generally these electron–hole pairs are easily recombined that reducing the photoresponse of semiconductors. However, the existing two phases make it possible for the photogenerated charges to migrate from anatase to rutile phases and to efficiently separate the photoinduced electron–hole pairs.

The developed single TiO_2 nanowire shows a low dark current of approximately pA level even at an applied voltage of 10 V, as shown in Fig. 4b. A significant increase in the current is observed under 254 nm UV light illumination (500 μW cm^{-2}) with a high photocurrent-to-dark current ratio of at approximately three orders of magnitude. The photocurrent of the sample annealed at 550 °C could reach up to 47 nA and 38 nA under 254 nm and 365 nm UV light at an applied voltage of 10 V, corresponding to a photo-dark current ratio of 760 and 600, respectively. For comparison, the photo-dark current ratio of the anatase (annealed at 500 °C) and rutile (annealed at 800 °C) TiO_2 nanowires are 160 and 1.1, respectively. The performance of the composite TiO_2 nanowires is comparable with other reported ZnO-based and TiO_2-based photodetectors.[34–38] Compared with reported flexible ZnO nanowires,[39,40] our TiO_2 network photosensor shows much better flexibility. For the ZnO photosensors, they can withstand a bending radius of 10 mm or 15 mm. But the photosensor would keep stable only after releasing the strain. In

our case, the photoresponse tests were measured while the sensor was under bending.

The flexibility of TiO_2 photodetector annealed at 550 °C was studied by bending to different curvature radii and repeated bending tests. It is noteworthy that the I–V characteristics keep linear and remain stable under UV light illumination, as shown in Fig. 5a. When bended to a radius from 100 to 5 mm, the responsivity shows a little decrease upon illumination at 254 nm. Even at the smallest curvature radius of 5 mm, the responsivity shows a high retention of 85% and 65% at 10 V and 1 V, respectively (Fig. 5c). The retention of responsivities at curvature radius of 100 mm and 10 mm was tested to be 96% and 78% during cycling under bending (Fig. 4b), respectively. This excellent flexible performance could be corresponding to the SEM results and visible bending tests in Fig. 2. As the TiO_2 nanowire could retain a continues nanostructure without any cracking, the electrical properties of them could also keep stable under bending. The response time of photodetector is another major issue for its practical application. Fig. 5d shows the response time of photodetector upon 254 nm illumination at 1 V and 10 V. When the applied voltage is 1 V, this response time decreases slightly under bending. With a higher voltage of 10 V excites the photosensor, this photoresponse time could be remained stable even after bending to a curvature radium of 5 mm. These results demonstrate the great mechanical flexibility and durability of this TiO_2 photodetector.
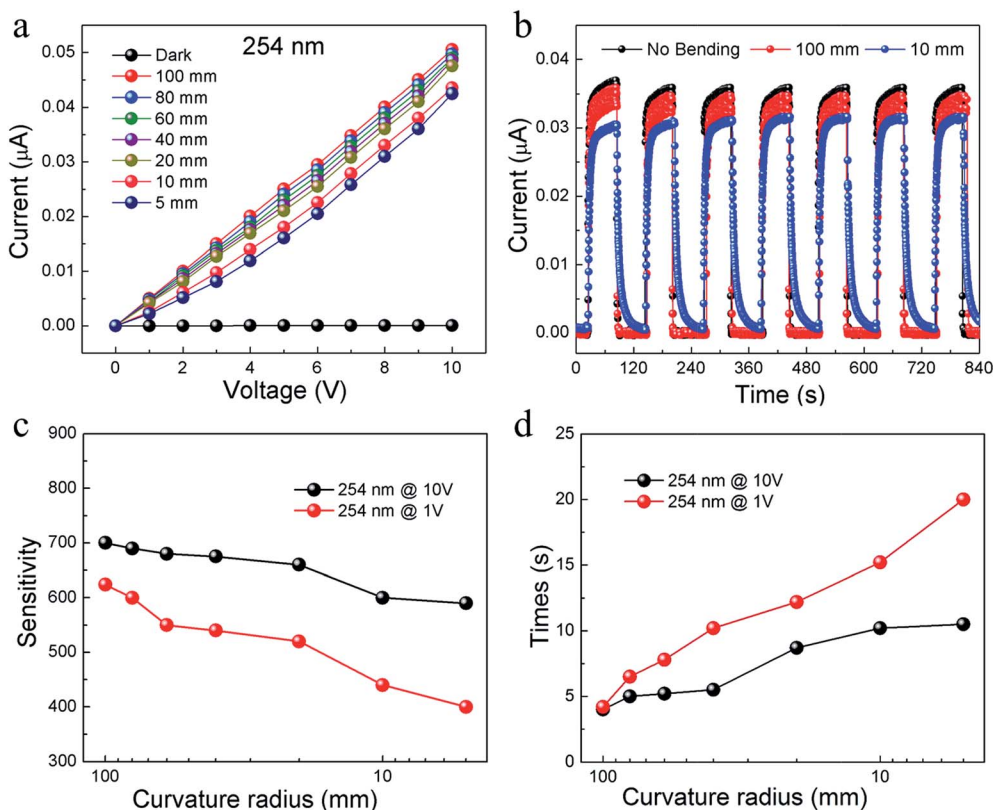

Fig. 5 (a) I–V curves of the flexible TiO_2 nanopaper photodetector annealed at 550 °C under dark or UV light illumination. (b) Photo-switching characteristics of the photosensor under dark and UV light. Plot of sensitivity (c) or response time (d) versus bending curvature radium of the photosensor under 254 nm at 1 or 10 V bias.
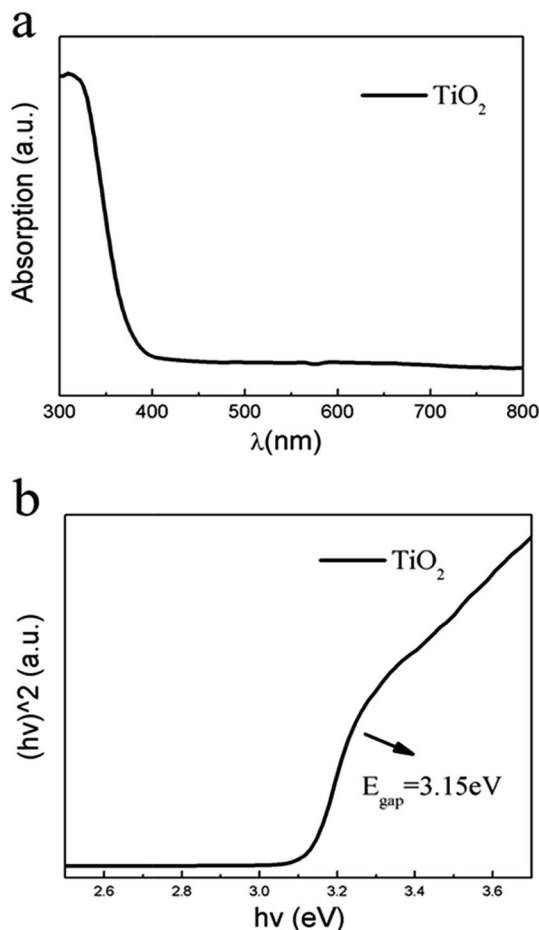
Fig. 6 (a) UV-visible diffuse reflection spectra of TiO_2 nanowires calcined at 550 °C, and (b) the corresponding plots of $(\alpha h\nu)^2$ *versus* photon energy $(h\nu)$.

To confirm the band gap of TiO_2 nanowires, Fig. 6a shows UV-vis diffuse reflection spectra of the TiO_2 nanowires annealed at 550 °C. The direct band gap of TiO_2 nanowires can be estimated by UV-vis diffuse reflection spectra using the following formation:[41] $(\alpha h\nu)^2 = A(h\nu - E_g)$ where α is the absorption coefficient, h is Planck's constant, ν is the photon frequency, A, a constant, and E_g is the optical band gap, respectively. Therefore, the band gap of the TiO_2 nanowires can be estimated from the data shown in Fig. 6b, corresponding to the energy band gap about 3.15 eV. This value is below that of anatase but higher than rutile TiO_2 shown in Fig. 4a, suggesting that the TiO_2 sample calcined at 550 °C consists of both anatase and rutile phases, corresponding to the XRD results.

4. Conclusions

In summary, a highly flexible TiO_2 photosensor was successfully fabricated *via* a facile electrospinning method. Not only did this photosensor show a high photo-dark current ratio of 760 and 600 under 254 nm and 365 nm UV light, respectively, but also exhibit excellent mechanical flexibility and durability. The possible mechanism is that the TiO_2 nanowires remain continuous and undergo nano-scaled deformation to relax the applied stress upon bending. Further observations under XRD demonstrate that the crystal structure of this sensor is composed of approximately 83% anatase and 17% rutile phases. The energy band gap of TiO_2 nanowebs is calculated to be 3.15 eV, which is a little lower than that of anatase but higher than rutile phase, corresponding to the XRD results. Both of these results could be correlated to the efficient electron–hole transfer between the two phases in the composites, which lead to the superior UV responsibility of our photosensor.

Acknowledgements

References

1 M. Y. Lee, J. Hong, E. K. Lee, H. Yu and H. Kim, *Adv. Funct. Mater.*, 2016, **26**, 1445.

2 X. Wang and G. Shi, *Energy Environ. Sci.*, 2015, **8**, 79.

3 N. Liu, H. Tian, G. Schwartz, J. B. H. Tok, T. Ren and Z. Bao, *Nano Lett.*, 2014, **14**, 3702.

4 Z. Alaie, S. M. Nejad and M. H. Yousefi, *Mater. Sci. Semicond. Process.*, 2015, **29**, 16.

5 H. Wu, W. Pan, D. Lin and H. Li, *J. Adv. Ceram.*, 2012, **1**, 2.

6 C. S. Boland, U. Khan, G. Ryan, S. Barwich, R. Charifou, A. Harvey, C. Backes, Z. Li, M. S. Ferreira, M. E. Mobius, R. J. Young and J. N. Coleman, *Science*, 2016, **354**, 1257.

7 W. Tian, C. Zhang, T. Zhai, S. L. Li, X. Wang, M. Liao, K. Tsukagoshi, D. Golberg and Y. Bando, *Chem. Commun.*, 2013, **49**, 3739.

8 H. Xue, W. Chen, C. Liu, X. Kong, P. Qu, Z. Liu, J. Zhou and L. Shen, *3rd IEEE International Conference on Nano/Micro Engineered and Molecular Systems*, 2008, **1**, 108.

9 Y. Chiba, A. Islam, R. Komiya, N. Koide and L. Han, *Appl. Phys. Lett.*, 2006, **88**, 223503.

10 C. Wu, C. Chao and F. Kuo, *Catal. Today*, 2004, **97**, 103.

11 R. Asahi, T. Morikawa, T. Ohwaki, K. Aoki and Y. Taga, *Science*, 2001, **293**, 269.

12 R. Daghrir, P. Drogui and D. Robert, *Ind. Eng. Chem. Res.*, 2013, **52**, 3581.

13 G. Jeong, J. Kim, M. Park, M. Seo, S. M. Hwang, Y. Kim, Y. Kim, J. H. Kim and S. X. Dou, *ACS Nano*, 2014, **8**, 2977.

14 Z. Sun, J. H. Kim, T. Liao, Y. Zhao, F. Bijarbooneh, V. Malgras and S. X. Dou, *CrystEngComm*, 2012, **14**, 5472.

15 F. H. Bijarbooneh, Y. Zhao, Z. Sun, Y. Heo, V. Malgras, J. H. Kim and S. X. Dou, *APL Mater.*, 2013, **1**, 32106.

16 J. Kim, D. Shi, K. Kong, Y. Heo, J. H. Kim, M. R. Jo, Y. C. Lee, Y. Kang and S. X. Dou, *ACS Appl. Mater. Interfaces*, 2013, **5**, 691.

17 J. Na, J. Kim, C. Park and E. Kim, *RSC Adv.*, 2014, **4**, 44555.

18 R. S. Chen, C. A. Chen, H. Y. Tsai, W. C. Wang and Y. S. Huang, *Appl. Phys. Lett.*, 2012, **100**, 123108.

19 L. Lin, L. Liu, K. Musselman, G. Zou and W. W. Duley, *Adv. Funct. Mater.*, 2016, **33**, 5979.

20 Z. Zhao, J. Tian, Y. Sang, A. Cabot and H. Liu, *Adv. Mater.*, 2015, **27**, 2557.

21 J. Zou, Q. Zhang, K. Huang and N. Marzari, *J. Phys. Chem. C*, 2010, **114**, 10725.

22 A. Pottier, C. Chaneac, E. Tronc, L. Mazerolles and J. Jolivet, *J. Mater. Chem.*, 2001, **11**, 1116.

23 S. Bakardjieva, J. Subrt, V. Stengl, M. J. Dianez and M. J. Sayagues, *Appl. Catal., B*, 2005, **58**, 193.

24 R. I. Bickley, T. Gonzalez-Carreno, J. S. Lees, L. Palmisano and R. J. D. Tilley, *J. Solid State Chem.*, 1991, **92**, 178.

25 A. Baji, Y. Mai, S. Wong, M. Abtahi and P. Chen, *Compos. Sci. Technol.*, 2010, **70**, 703.

26 H. Wu, D. Kong, Z. Ruan, P. Hsu, S. Wang, Z. Yu, T. J. Carney, L. Hu, S. Fan and Y. Cui, *Nat. Nanotechnol.*, 2013, **8**, 421.

27 C. Niu, J. Meng, X. Wang, C. Han, M. Yan, K. Zhao and X. Xu, *Nat. Commun.*, 2015, **6**, 1.

28 L. Zhu, X. Gu, F. Qu, J. Zhang and C. Feng, *J. Am. Ceram. Soc.*, 2013, **96**, 3183.

29 J. Cheng, H. Li, S. Huang and W. Pan, *J. Am. Ceram. Soc.*, 2014, **8**, 2372.

30 J. Cheng, Y. Wang, Y. Xing, M. Shahid and W. Pan, *RSC Adv.*, 2017, **7**, 15330.

31 W. E. Teo and S. Ramakrishna, *Nanotechnology*, 2006, **17**, 89.

32 D. Yang, H. Liu, Z. Zheng, Y. Yuan, J. Zhao and E. R. Waclawik, *J. Am. Chem. Soc.*, 2009, **131**, 17885.

33 T. Kawahara, Y. Konishi, H. Tada, N. Tohge, J. Nishii and S. Ito, *Angew. Chem.*, 2002, **114**, 2935.

34 C. Soci, A. Zhang, B. Xiang, S. A. Dayeh, D. P. R. Aplin, J. Park, X. Y. Bao, Y. H. Lo and D. Wang, *Nano Lett.*, 2007, **7**, 1003.

35 C. Lu, S. Chang, S. Chang, C. Lee and C. Kuo, *Appl. Phys. Lett.*, 2006, **89**, 153101.

36 G. Liu, N. Hoivik and K. Wang, *Electrochem. Commun.*, 2013, **28**, 107.

37 T. Tsai, S. Chang, W. Weng, C. Hsu, S. Wang, C. Chiu, T. Hsueh and S. Chang, *J. Electrochem. Soc.*, 2012, **159**, J132.

38 W. Zheng, X. Li, G. He, X. Yan, R. Zhao and C. Dong, *RSC Adv.*, 2014, **4**, 21340.

39 Z. Zheng, L. Gan, H. Li, Y. Ma, Y. Bando, D. Golberg and T. Zhai, *Adv. Funct. Mater.*, 2015, **25**, 5885.

40 Y. Wang, M. Shahid, J. Cheng, H. Nishijima and W. Pan, *Nanotechnology*, 2017, **28**, 155202.

41 P. Singh, A. Kumar, A. Kaushal, D. Kaur, A. Pandey and R. N. Goyal, *Bull. Mater. Sci.*, 2008, **31**, 573.